Evaporation Behaviour of a Thinning Liquid Film in a Spin Coating Setup: Comparison Between Calculation and Experiment

José Danglad-Flores[a], Stephan Eickelmann[a], Hans Riegler[a,]

[a] *Max-Planck-Institut für Kolloid- und Grenzflächenforschung, D-14476 Potsdam-Golm, Germany*

Abstract

We present and analyze comprehensive measurements of the evaporation behavior, E, of a thinning liquid film during a hydrodynamic - evaporative spin coating experiment. E, ω (the rotation speed), and ν (the liquid viscosity) are the main control parameters of the process. The entire film thinning process can be described theoretically quite well if these parameters are known. Values of ν are easily accessible in advance (calculations, literature values, measurements). Values for E can essentially not be found in the literature. They are hard to measure and specific for the experimental conditions. There is also no generally accepted strategy to calculate E. Our experimental results are compared with a theoretical prediction for E based on ideas by Bornside, Macosco, and Scriven, which were presented long ago. Their approach was never tested experimentally. Theory and experiment agree well for many solvents and different ω. This approach permits *in advance* the quantitative calculation of the evolution of the entire hydrodynamic-evaporative film thinning process. We also derive a general formula to predict ab initio, with literature data only, the amount of final deposit (film thickness) of solute in the case of spin coating mixtures of volatile solvents and nonvolatile solutes.

Keywords: Evaporation, Spin Coating, Spin Casting, Thin Liquid Films, Final Film Thickness, Final Deposition.

1. Introduction

Spin coating is widely used in research and in industrial applications to prepare thin planar films on substrates [1]. In the process, a small amount of liquid is deposited on a rotating planar substrate and spread into a planar film by centrifugal forces. The liquid may be a melt or a solution. Here we will focus on hydrodynamic-evaporative spin coating i.e., spin coating of mixtures of volatile solvents and nonvolatile solutes. After evaporation of the volatile components this process results in the deposition of a thin film of mainly solute [2]. Typically this solute film is the main purpose of the process. The thickness of the solute film (the solute coverage) can be adjusted through the process parameters. The most relevant parameters are 1.) the liquid viscosity [3], 2.) the solute concentration [4], 3.) the rotation speed [5, 6], and 4.) the evaporation behavior of the liquid [2, 7–9].

The thinning of the liquid film and the spatio-temporal evolution of the solute/solvent composition during hydrodynamic - evaporative spin coating have been analyzed in some detail [10–14]. Meanwhile the process is understood quite well [15–17] and if the physico-chemical process parameters are known, in many cases, the final solute coverage can be predicted. In fact, aside from the evaporation

Email address: hans.riegler@mpikg.mpg.de; telephone:+49 331 567 9236 (Hans Riegler)

rate, all the other relevant spin coating parameters can be obtained rather easily, e.g., from literature or from independent measurements. For instance, the density and viscosity of the solvent/solute mixture can be measured or obtained (calculated) from literature data. The rotation speed can be adjusted.

Alas, reliable values for evaporation rates under spin coating conditions cannot be found in the literature. They are considered to be rather specific for the experimental conditions (geometry of the spin coating setup, rotation speed, etc.). Therefore, it has been suggested to measure the evaporation rate of a specific solvent for a specific spin coating configuration [18, 19]. This evaporation rate can then be used to calculate the outcome of spin coating processes with the same setup and solvent, but otherwise different process parameters. The relevant evaporation rate can be derived for instance, from the final solute coverage resulting from a "calibration" spin coating experiment [2, 16]. This approach is useful. Nevertheless, it is still desirable to know/calculate the evaporation rate in advance without the necessity of a "calibration" experiment. Thus, one would gain for instance substantial flexibility to preselect suitable solvents to achieve a desired spin coating result.

Already some time ago, Bornside, Macosco, and Scriven (abbreviated in the following as "BMS") proposed how to calculate the evaporation behavior of volatile liquids in a spin coating configuration [7, 20, 21]. For the calculation only readily accessible literature and process parameter data are necessary. Up to now this theoretical approach has never been tested/confirmed thoroughly by experiment. Presumably this is the case, because 1.) reliable experimental evaporation data were not available and 2.) a concise theoretical description of the spin coating process was not existing until recently. Indeed, evaporative film thinning in spin coating configurations has been measured [14, 22–25]. However, until recently it was not clear how meaningful these data were. For instance, it has been discussed whether there exists something like a "simple" evaporation rate [26, 27]. It was unclear how much the increase of the solute concentration during evaporative film thinning might affect the evaporation rate itself (e.g. via a "skin formation" [28]) and thus modify the film thinning process and in particular the resulting final solute deposition [29]. Also, the impact of film dewetting (hole formation) during film thinning (in particular in the late stages of film drying) was not known [30].

With on-line imaging of the film thinning during the spin coating process it is possible to investigate the film thinning behavior with high precision [17, 30]. We applied this experimental approach and in the following we will present precise experimental data on the evaporation behavior derived from the film thinning. The results will be analyzed in view of the predictions of the BMS approach. We will address in particular whether the BMS theory can be used to quantitatively describe the evaporative contribution to the liquid film thinning in a spin coating process. In addition we will discuss in which cases it is possible to apply this approach for solvent/solute mixtures. Last not least we will show how the new insights can be used to predict the final solute coverage, i.e., the main purpose of most spin coating processes.

2. Materials and Methods

Chemicals.–Toluene ("TOL", 99.9 %), methylcyclohexane (99.5%), dimethylformamide (99 %), and n-nonane (99.8 %) were from Sigma Aldrich. Tetrahydrofuran ("THF", $\geq$ 99.5 %) was from VWR. Ethylacetate ("EA", 99.5 %)

was from Chemsolute. Chloroform ("CH", $\geq$ 99.8 %) and n-octane (99 %) were from MERCK. n-heptane $\geq$ 99 % was from Fluka. n-decane (99 %) was from Alfa Aesar. Water ("W", Milli−Q Pure Water System) had a resistivity of 18 MΩcm. Block copolymers of polystyrene and polymethylmethacrylate (PS-b-PMMA, M x 10^3= 55-b-22, $\rho = 945 kg/m^3$) were from from Polymer Source Inc.

Substrates.–As substrates served silicon wafer pieces of $\approx$ 2 cm x 2 cm with natural oxide surfaces (oxide layer thickness $\approx$ 2 nm) or with artificial oxide layers of (50 $\pm$ 1) nm thickness. In both cases the surface roughness was $\approx$ 0.5 nm.

Substrate surface preparation.–The substrates were first cleaned in an ultrasonic bath by a sequence of immersions (for 10 *min* each) in: 1.) de-ionized water, 2.) ethanol, 3.) acetone, 4.) ethanol, and 5.) de-ionized water. In a second cleaning step they were immersed for 30 min in piranha solution (H_2O_2(35 %)/H_2O(65 %) and H_2SO_4 (96 %), 1:3 volume ratio). Finally they were again immersed and sonicated for 10 min in de-ionized H_2O and stored therein. Just before use they were dried by blowing with dry N_2 (purity: 5.0).

Optical imaging.–For the in-situ observation of the spin coating process, a modified optical microscope (Axio Scope A1 from Zeiss) was used. The light source was a blue diode laser (6 W, 445 nm, LDM-445-6000, LASERTACK, de-speckled by a combination of liquid light guide and a rotational diffusor). Microscopy was performed from the top in interference enhanced reflection mode [31]. A high speed monochromatic camera (1000 fps) and suitable image triggering and processing provided single frames during the film thinning [32]. Interferometric data (brightness variations during film thinning) revealed the film thinning behaviour [33] (for more details see also Supplement).

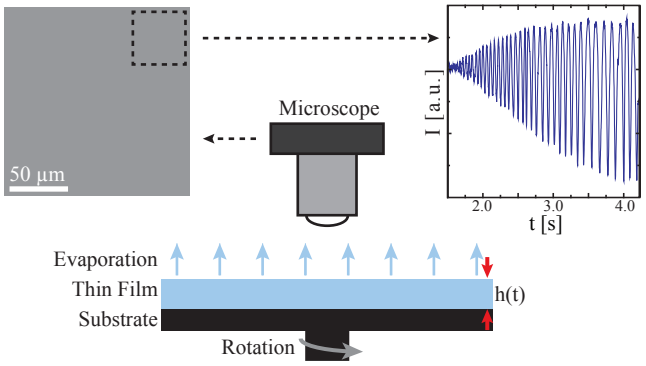

Figure 1: Experimental setup to measure the hydrodynamic-evaporative thinning of a volatile liquid film in a spin coating configuration. The sample surface is imaged via reflection microscopy i.e., with monochrome illumination from the top (through the lens). The interference of the light reflected from the surface of the continuously thinning liquid film and from the interface between the film and the substrate surface modulates the intensity of the reflected light as indicated. The time evolution of the film thickness can be derived from these intensity modulations with great precision. More technical details on the experimental setup (synchronization of the frame rate with the sample rotation, background subtraction, etc.) can be found in [30] and in the Supplement.

Spin coating.–The home-made spin coater allowed a precise adjustment of the rotation speed. The substrate holder was a planar, round Teflon disk with a diameter of 3 cm. It had a small hole in the center, where a negative pressure could be applied to fix the substrates. The combination of spin coater and microscope was not encased in closed box. Instead, the rotating sample surface was exposed to the normal laboratory air convection environment. There was no artificial, extra air flow directed towards the substrate surface. There was also no strong environmental air flow, e.g. due to air conditioning or a chemical hood. The microscope and the spin coater were arranged as sketched in Figure 1.

In the experiment a drop (0.2 mL) of the liquid is placed on the solid, planar substrate, which is already rotating at a constant speed, ω. After its deposition, the liquid drop rapidly forms a planar film due to the combination of centripetal and viscous forces [3]. Due to outward liquid flow and/or spin off at the substrate perimeter, the height, h, of this liquid film is continuously decreas-

ing ($h = h(t)$). With volatile liquids, evaporation also contributes to film thinning. Because viscous shear forces increase rapidly if the film gets thinner evaporative liquid losses increasingly dominate film thinning. For sufficiently thin films the outward liquid flow practically ceases and film thinning only occurs due to evaporation. This range of essentially purely evaporative film thinning reveals the evaporation rate, E [14–16, 18], with a linear decrease of the film thickness:

$$dh/dt = -E. \tag{1}$$

E can be determined with great precision with the setup depicted in Figure 1 in combination with Equation (1). In the observed film thinning behavior the range of purely evaporative thinning can be identified easily, because the transition between the (nonlinear) thinning driven by lateral liquid flow and the linear thinning dominated by evaporation is rather well defined and can be measured experimentally. The transition occurs at (and defines) the so-called transition film height, h_{tr}. The theoretical analysis of hydrodynamic-evaporative film thinning [15, 34] shows that h_{tr} is related to E, ν (viscosity) and ω (rotational velocity) according to:

$$h_{tr} = \left(\frac{3E\nu}{2\omega^2}\right)^{1/3}. \tag{2}$$

The transition height, h_{tr}, is *the* key process parameter, because together with the solute concentration it can be used to calculate the final deposit of the solute (see discussion section).

As mentioned above, the evaporation rate, E, can be determined directly from the linear section of the thinning curve as described above by Eq.(1). For this publication we derived E by fitting the entire thinning curve with the theoretical model presented by Karpitschka et *al* [15]. This *zero-order* approach assumes that E and ν remain constant during the whole process. Detailed theoretical and experimental investigations show that this approach describes the thinning curve with excellent precision for the experimental conditions applied here (pure solvents and mixtures with low solute concentrations). In particular, it effortless yields precise values for E. In any case, fitting the complete curve results within the measurement errors in the same values for E as those obtained directly from the slope of the thinning curve in the linear range.

3. Theoretical calculation of E

Some time ago Bornside, Macosko, and Scriven presented a theoretical description of the steady state evaporation behavior of thin volatile films in a spin coating configuration [7, 20, 21, 35]. They predict an evaporation rate, E, with[1]:

$$E = k\frac{\rho_{vap}}{\rho_{solv}}(x_{solv} - x_{solv,\infty}). \tag{3}$$

Here, ρ_{solv} is the solvent density in its liquid phase and ρ_{vap} is its density in the vapor phase. x_{solv} and $x_{solv,\infty}$ are the solvent mass fractions in the liquid phase and faraway from the liquid in the vapor phase, respectively. k is the mass transfer coefficient.

Assuming Raoult's law to describe the vapor-liquid equilibrium of the solvent and the ideal gas law to estimate its

[1] In contrast to the theoretical approach taken in this report, which starts with pure solvents and modifies the findings to solutions, BMS focused in their theoretical description right away on the evaporation rates of polymer solutions. They assumed, for instance, nonlinear changes of the viscosity and of the partial pressure of the solvent during the process. Their approach is complicated and not easily comprehensible. This limits its value, in particular for users, who want to apply spin coating without caring about its physicochemical background. In hindsight, the method applied by BMS is absolutely apprehensible. Detailed experimental data about the film thinning were barely available at their time, not to mention a consistent theory on spin coating, which does exist meanwhile [15].

density [7, 20] Eq.(3) can be written as:

$$E = k \left(\frac{P^*_{solv} M_{solv}}{\rho_{solv} R_g T} \right) (x_{solv} - x_{solv,\infty}). \quad (4)$$

P^*_{solv} is the vapor pressure of the pure solvent and M_{solv} is its molecular weight. R_g is the ideal gas constant and T is the temperature.

According to Bornside, Macosco, and Scriven for a planar plate rotating at speed ω the mass transfer coefficient k can be replaced leading to:

$$E = \left(\frac{c D_{solv,air} \omega^{1/2}}{\nu_{air}^{1/2}} \right) \left(\frac{P^*_{solv} M_{solv}}{\rho_{solv} R_g T} \right) (x_{solv} - x_{solv,\infty}). \quad (5)$$

The constant c is a function of the Schmidt number Sc with $c = 0.386 \cdot \mathrm{Sc}^{0.462}$ and $Sc = \nu_{air}/D_{solv,air}$ [6]. $D_{solv,air}$ is the diffusion coefficient of the solvent ($solv$) in air (air) and ν_{air} is the kinematic viscosity of air.

With the approximation $c = 0.386 \cdot \mathrm{Sc}^{0.462} \approx 0.4 \cdot (\nu_{air}/D_{solv,air})^{1/2}$, Eq. (5) can be simplified to:

$$E \approx 0.4 \cdot D^{1/2}_{solv,air} \omega^{1/2} \left(\frac{P^*_{solv} M_{solv}}{\rho_{solv} R_g T} \right) (x_{solv} - x_{solv,\infty}). \quad (6)$$

For pure solvents $x_{solv} = 1$ and $x_{solv,\infty} = 0$, because the solvent concentration in the air far away from the evaporating surface can be neglected. Therefore $(x_{solv} - x_{solv,\infty}) = 1$. Accordingly, Eq. (6) can be simplified further:

$$E \approx \frac{0.4 \cdot D^{1/2}_{solv,air} \omega^{1/2} P^*_{solv} M_{solv}}{\rho_{solv} R_g T}. \quad (7)$$

This is an important result, because all the data necessary to calculate E via Eq. (7) are either available from literature or given by the experimental conditions.

4. Experimental Results

4.1. Evaporation rates for different liquids

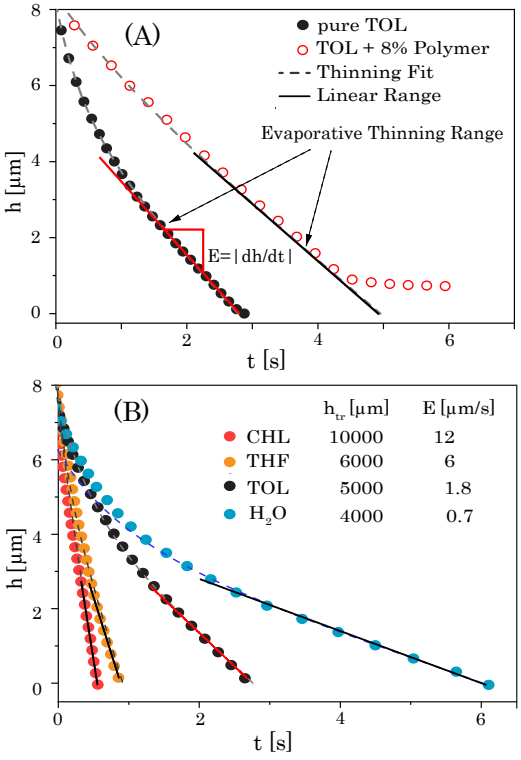

Figure 2: Experimentally measured thinning curves (ω=2000 rpm). The solid lines indicate the linear slope range of the purely evaporative region with $dh/dt = -E$. Panel (A): Pure toluene (TOL) and a solution of toluene with 8 % PS-b-PMMA (MW:55k-b-22k). For better visualization the curves are shifted laterally on the time axis. Panel (B): chloroform (CHL), tetrahydrofuran (THF), toluene (TOL), and water (H_2O, 26 °C, relative humidity 40 %). The dashed lines are the theoretical fit thinning curves according to the "zero-order" model.

Fig. 2−A depicts examples of a thinning curve of a pure solvent (toluene) and of a solution of this solvent with 8% PS-b-PMMA (MW:55k-b-22k). For better visualization the curves are shifted laterally on the time axis. The data were measured with the setup depicted in Figure 1. Fig. 2−B presents examples of experimentally observed thinning curves for several pure solvents.

The region of film thinning dominated by evaporation can easily be identified in all cases. It is the range where the film height decreases linearly, ending with the bare substrate (h=0) for the pure solvents. In the case with the solution containing a nonvolatile component, the decrease

ends with a final deposit of film thickness, $h(t \to \infty) = h_f$. The solid lines show the slope of the purely evaporative region with $dh/dt = -E$ according to Eq. (1). The interpretation of the data with respect to the evaporation behavior is corroborated by the analysis of the entire thinning curve. The dashed lines are theoretical fits to the experimental data according to the scenario of hydrodynamic-evaporative film thinning as described in the supplement and in the literature [15]. In short, this scenario takes into account both, hydrodynamic and evaporative thinning. It assumes ("zero-order theory") only a volatile liquid and neglects the impact of the solute concentration (and changes thereof during the film thinning) on the evaporation behavior. Despite this supposedly rather crude assumption, the agreement between experiment and theory remarkably is good (this is the case even for higher order corrections see [16, 17]).

4.2. Evaporation rates for different rotation speeds

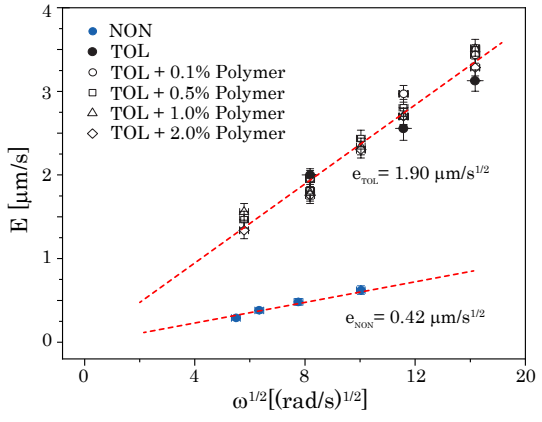

Figure 3: Experimentally measured evaporation rates, E, as function of the square root of the sample rotation, $\omega^{1/2}$. Data are shown for pure n-nonane (NON), pure toluene (TOL), and for various solutions of PS-b-PMMA (MW:55k-b-22k) in toluene (the polymer concentrations are given in mass percentage). The dashed lines show linear fits with slopes indicating the speed-independent evaporation rates e_{TOL} as defined by Eq. (8).

Figure 3 shows evaporation rates, E, as function of the square root of the rotational speed, $\omega^{1/2}$. Data are presented for pure solvents (nonane and toluene) and for solutions of toluene with various concentrations of PMMA. The dashed lines are fits to the data supporting the validity[2] of Eq. (7) with [18]:

$$E \propto \omega^{1/2}. \tag{8}$$

For a better comparison of the data at various rotation speeds it is convenient to re-scale the evaporation rates and to define a speed-independent evaporation rate, e, by rewriting Equation (7) accordingly:

$$e = \frac{E}{\omega^{1/2}} \approx \frac{0.4}{R_g T}\left(\frac{D_{solv,air}^{1/2} P_{solv}^{*} M_{solv}}{\rho_{solv}}\right). \tag{9}$$

.

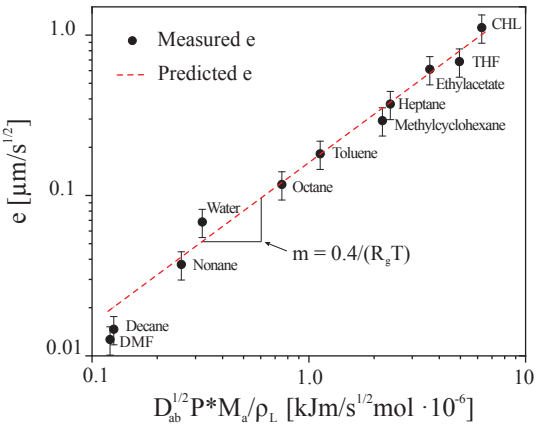

Figure 4: Experimentally measured speed-independent evaporation rates, e, for various solvents as function of the pure solvent properties $D_{ab}P^{*}M_a/\rho_L$ (see Appendix, Table 1). The dashed line shows a linear fit (Pearson coefficient = 0.996) through the origin. Its slope is 1.6×10^{-4} mol/J.

Figure 4 presents evaporation data for many different pure solvents. The data are plotted according to Eq. (9) with the physico-chemical data for the different systems obtained from literature (see appendix). Motivated by Eq. (9) the dashed straight line in Figure 4 has a slope

[2]For simplicity it is assumed for the fits that $E(\omega = 0) = 0$. The experimental data are not accurate enough to conclude/predict with sufficient significance by extrapolation the (small) evaporation rates for $E(\omega \to 0)$.

of $0.4/(R_gT)$ with $T = 26°C$, the experimentally applied temperature.

5. Discussion

5.1. General remarks

Evaporation rates in a spin coating configuration, $E(\omega)$, were measured for different rotation speeds, different solvents, and various solvent/solute mixtures by direct observation of the film thinning. The measurements via on-line imaging show that the evaporating liquids form closed and planar films throughout the entire film thinning process. Thus it is assured that the evaporative film thinning agrees with the scenario assumed for a typical spin coating process as it is described by the corresponding theory [15].

It is observed that the evaporation rates are proportional to $\omega^{1/2}$. This behavior and the absolute numbers measured for E are in good quantitative agreement with a theoretical prediction published some time ago by Bornside, Macosko, and Scriven [7, 20]. This means that E can be calculated directly from literature data of the solvent properties and from readily available process parameters. More so, because all the other process parameters are also accessible in advance, it means that it is possible to calculate *ab inito* the entire film thinning in the course of the spin coating process including its result, the deposition of the solute.

5.2. Validity and limitations of the approach

Quite remarkable, the technical specifications of the spin coating setup, such as for instance the size/diameter of the substrate, are not taken into account by the BMS approach. It is rather unlikely that the technical conditions of our setup just by chance lead to the observed quantitative agreement between theory and experiment. Our conditions (see Materials and Methods) were: 1.) sample exposed to a normal laboratory air environment without artificial air flow; 2.) substrate dimensions of a few *cm* in diameter; 3.) deposition of an excess volume of the liquid on the sample already rotating at a fixed speed. It can be assumed, that under similar spin coating conditions the evaporation rates can also be calculated quite accurately via the BMS approach.

Which aspects of different technical implementations of spin coating setups may or may not have an influence on the validity of the presented calculation of E can be guessed from the line of argumentation following Equations (3) through (7). According to Eq. (3) the evaporation rate depends on the difference of the vapour pressures, $x_{solv} - x_{solv,\infty}$, and on the transfer coefficient, k. For pure solvents, $x_{solv} = 1$. This assumption still holds with good approximation (i.e., error $\leq 10\%$) also for solutions, as long as the *mass* concentration of the solute is $\leq 10\%$ [16, 17]. The assumption of $x_{solv,\infty} = 0$ is also reasonable if the environmental vapor pressure of the solvent is low. The content of the first round bracket of Eq.(5) means that k depends on the air flow conditions close to the substrate surface created by the process itself (sample rotation). With rotational speeds typically applied in spin coating (e.g., from 500 *rpm* to 3000 *rpm*), this means induced air flow speeds near the sample surface in the range of 1 m/s and more (= perimeter rotational speeds for sample sizes of a few *cm* at 10 *rps*). The size of the sample does not appear in Equations (3) through (7) because its impact on k is generally considered rather weak[36–38]).

In agreement with our results, this means that the presented calculation of E is reasonable, if the spin coating setup is *not* placed within a closed compartment of small (vapour) volume (i.e., the environmental solvent va-

por pressure, $x_{solv,\infty}$ remains small). The calculation is also applicable, if there is no external air flow exceeding speeds of 0.1-0.2 m/s [39] and aiming directly at the substrate surface. This means flow from air conditioning or a chemical hood may or may not cause a problem. It depends on where exactly the spin coater is positioned (for instance, placed within the hood closer to the rear corner is okay, whereas a location in front next to a nearly closed door may cause a problem). Sample sizes between 1 and 10 *cm* in diameter should be okay.

With liquid mixtures of two or more different volatile components the evaporation behavior and thus the film thinning behavior may not be described correctly by assuming a (constant) evaporation rate calculated with (the approach leading to) Eq. (7). Even if the calculation of E with an appropriately modified (for mixtures) Eq. (7) yields a correct evaporation rate for thick planar films, Marangoni effects may influence the thinning behavior of thin films. They may cause surface undulations in the late stages of film thinning and thus, for instance film rupture. Last not least, miscibility gaps may affect E and ν.

Another aspect has to be considered for solutions of volatile solvents and nonvolatile solutes. Even with small solute concentrations, the viscosity of the solution can be very different to the viscosity of the pure solvent. In this case the film thinning process can be described quantitatively quite well by taking into account the viscosity of the *solution* rather than the *solvent* [16, 17]. The result will be correct if the true initial viscosity (of the solution), ν, and the applied ω, is taken to calculate/predict the film thinning behavior. For the evaporation rate it is sufficient take an E, which is calculated with Eq. (7) by assuming the pure solvent. In this case E of the pure solvent is acceptable, because the evaporation rates of pure solvent and solution are quite similar as long as the solute concentration does not exceed 10-20 % due to evaporative enrichment. Of course, in the very late stages of film thinning the deviation between experiment and calculation becomes significant, because solute deposition is not explicitly taken into account in modelling the thinning of the film in the zero-order approach. Nevertheless, the amount of solute deposition can be calculated, because it is determined by the conditions at the early stages of the hydrodynamic-evaporative film thinning. The evaporation rate can still be calculated with reasonable precision assuming the pure solvent properties. If the (measurable) true initial solute viscosity is taken into account, it is possible to quite accurately predict the amount of final solute as will be shown in the following.

5.3. Estimation of the solute deposition

The final solute film thickness can be calculated with the spin coating parameters via the transition height, h_{tr} (see Eq.(2)) as follows [15–17]:

$$h_f \approx x_0 \cdot h_{tr}. \tag{10}$$

This equation assumes identical densities of the solvent and the solute and x_0 denotes the volume ratio between solute and solvent in the initial (weighing in) solution.

With different densities of solvent, ρ_{solv}, and solute, ρ_{solute}, Eq. (10) has to be modified:

$$h_f \approx x_0 \cdot \frac{\rho_{solv}}{\rho_{solute}} \cdot h_{tr}. \tag{11}$$

If the solute concentration is given as c_0 i.e., as an entity per volume (e.g., moles or particles per volume), deposition leads to a final coverage of the solute in entity per area, Γ_0:

$$\Gamma_f \approx c_0 \cdot \frac{\rho_{solv}}{\rho_{solute}} \cdot h_{tr}. \quad (12)$$

It should be noted that ρ_{solute} denotes the *average* density of the solute. This is important, for instance, in the case of metal nanoparticles coated with a shell of organic molecules (see example in the Supplement). In this case ρ_{solute} results from the weight of the particle core plus its shell divided by the volume of the entire particle (core and shell).

5.4. The final "master" equation

The combination of Eq.(11) or Eq.(12) with Eq.(7) yields a general "master" formula to predict ab initio the final film thickness:

$$h_f \approx 0.85 \cdot x_0 \cdot \frac{\rho_{solv}}{\rho_{solute}} \cdot \left[\frac{\nu D_{solv,air}^{1/2} P_{solv}^* M_{solv}}{\omega^{3/2} \rho_{solv} R_g T} \right]^{1/3}. \quad (13)$$

or the final coverage:

$$\Gamma_f \approx 0.85 \cdot c_0 \cdot \frac{\rho_{solv}}{\rho_{solute}} \cdot \left[\frac{\nu D_{solv,air}^{1/2} P_{solv}^* M_{solv}}{\omega^{3/2} \rho_{solv} R_g T} \right]^{1/3}. \quad (14)$$

The assumptions leading to Eqs.(11) and (12) indicate an accuracy of about ±10%. Assuming similar margins for Eq.(7) based on the experimental results presented in Fig. 4, suggests an accuracy of typically ±(20)% or better for the final master Eqs.(13) and (14). This is consistent with the experimental data of Figs. 3 and 4.

In the Supplement we present two examples, which confirm our assumptions regarding the accuracy of the ab initio predictions made by Eqs.(13) and (14). We present predictions based on cases of experiments performed by other groups concerning 1.) nanoparticle monolayer deposition [40] and b) deposition of precursor for in situ polymerized films [41]. In the examples we take the relevant spin coating data from the information given in the publications[3]. Together with these data, literature data and Eqs.(13) (or (14)) we can reproduce the described experimental findings quite well.

6. Summary and Conclusion

Hydrodynamic-evaporative spin coating is the process of the evolution of a planar, continuously thinning film of a (partially) volatile liquid on a rotating substrate. Recently this process has successfully been analyzed quantitatively and described theoretically. The film thinning behavior is essentially determined by three control parameters: 1.) the evaporation rate, E, 2.) the liquid viscosity, ν, and 3.) the rotation speed, ω. If the liquid is a solution of a volatile solvent and a nonvolatile solute, a final deposit of the solute remains after evaporation of the solvent. The amount of final deposit can be calculated from a fourth parameter, x_0, the solute concentration of the solution at the beginning of the process.

Three of these parameters, ω, ν , and x_0, are readily available prior to the spin coating process. They can either be adjusted, easily measured, or obtained (calculated) from literature data. Values for E, on the other hand, are not readily available for several reasons. It is not easy to measure E under different spin coating conditions. Prior to the recent progress in understanding the process theoretically in depth, the complicated film thinning process with its time-dependent combination of evap-

[3]Many spin coating experiments are described in the literature, mostly to prepare films of specific thicknesses, composition, etc., to be used for certain applications. However, it is very hard to find publications, which contain all the relevant parameters necessary to unambiguously reproduce the experiments (meaning: which completely specify the process as we define and investigated it in previous publications).

orative and hydrodynamic contributions suggested that E changes during the process. E was also considered to be rather specific for the experimental setup. Not the least because of these reasons, there was no generally accepted approach on how to calculate E.

Yet, already some time ago Bornside, Macosco, and Scriven suggested a way to calculate E. Up to now, their proposal has never been adapted appropriately and tested by experiment. We measured evaporation rates, E, of many different volatile solvents and mixtures of volatile solvents and non-volatile solutes under different spin coating conditions and analyze them in view of the proposal by Bornside, Macosco, and Scriven. We find that their theoretical calculation of E agrees remarkably well with our measured E for many different solvents and spin coating conditions. We combined their approach with the recently available theoretical description of spin coating. Thus the entire spin coating process can be calculated/modelled quantitatively in advance. This is of great practical importance, because in the case of spin coating solutions containing nonvolatile solutes, this solute is deposited in the course of the process. In most cases this deposition of the solute is the main purpose of the spin coating process. Not the least, this is because through the variation of the process parameters the amount of solute deposition can be controlled and adjusted within wide margins. We present a "master" formula to calculate in advance the final solute deposit. This ab inito calculation is solely based on data readily available prior to the process. Thus the desired solute coverage can be optimized/adjusted in advance.

Acknowledgements—Thanks to Reinhard Lipowsky for institutional support. JDF was funded by the DAAD and DFG through the IRTG 1524. JDF thanks for his training the GISDE, Universidad de Oriente, Venezuela.

[1] R. G. Larson, T. J. Rehg, Spin Coating, Springer Netherlands, Dordrecht, 1997, pp. 709–734.

[2] D. Meyerhofer, Characteristics of resist films produced by spinning, Journal of Applied Physics 49 (7) (1978) 3993–3997.

[3] A. G. Emslie, F. T. Bonner, L. G. Peck, Flow of a viscous liquid on a rotating disk, Journal of Applied Physics 29 (5) (1958) 858–862.

[4] B. Washo, Rheology and modeling of the spin coating process, IBM Journal of Research and Development 21 (2) (1977) 190–198.

[5] W. Cochran, The flow due to a rotating disc, in: Mathematical Proceedings of the Cambridge Philosophical Society, Vol. 30, Cambridge University Press, 1934, pp. 365–375.

[6] F. Keith, J. Taylor, J. Chong, Heat and mass transfer from a rotating disk, Tech. rep., DTIC Document (1958).

[7] D. Bornside, C. Macosko, L. Scriven, Spin coating of a pmma/chlorobenzene solution, Journal of the Electrochemical Society 138 (1) (1991) 317–320.

[8] J. Coca, J. Bueno, R. Alvarez, Gaseous diffusion coefficients by the stefan-winkelmann method using a polymer-solvent mixture as evaporation source, Ind. Eng. Chem. Fundam. 19 (2) (1980) 219–221.

[9] D. B. Hall, P. Underhill, J. M. Torkelson, Spin coating of thin and ultrathin polymer films, Polymer Engineering & Science 38 (12) (1998) 2039–2045.

[10] B. Reisfeld, S. Bankoff, S. H. Davis, The dynamics and stability of thin liquid films during spin coating. i. films with constant rates of evaporation or absorption, Journal of applied physics 70 (10) (1991) 5258–5266.

[11] D. P. Birnie III, M. Manley, Combined flow and evaporation of fluid on a spinning disk, Physics of Fluids 9 (4) (1997) 870–875.

[12] E. Momoniat, T. Myers, A new solution for the rotation-driven spreading of a thin fluid film, International Journal of Non-Linear Mechanics 41 (2) (2006) 192–199.

[13] V. Cregan, S. B. O'Brien, Extended asymptotic solutions to the spin-coating model with small evaporation, Applied Mathematics and Computation 223 (2013) 76–87.

[14] Y. Mouhamad, P. Mokarian-Tabari, N. Clarke, R. Jones, M. Geoghegan, Dynamics of polymer film formation during spin coating, Journal of Applied Physics 116 (12) (2014) 123513.

[15] S. Karpitschka, C. M. Weber, H. Riegler, Spin casting of dilute solutions: Vertical composition profile during hydrodynamic-evaporative film thinning, Chemical Engineering Science 129

(2015) 243–248.

[16] J. Danglad-Flores, S. Eickelmann, H. Riegler, Deposition of polymer films by spin casting: A quantitative analysis, Chemical Engineering Science 179 (2018) 257 – 264.

[17] J. Danglad-Flores, K. Eftekhari, A. G. Skirtach, H. Riegler, Controlled deposition of nanosize and microsize particles by spin-casting, Langmuir 35 (9) (2019) 3404 – 3412.

[18] D. E. Haas, J. N. Quijada, S. J. Picone, D. P. Birnie, Effect of solvent evaporation rate on skin formation during spin coating of complex solutions, Sol-Gel Optics V 3943 (2000) 280–284.

[19] D. Haas, Predicting the uniformity of two-component, spin deposited films.

[20] D. E. Bornside, R. A. Brown, P. W. Ackmann, J. R. Frank, A. A. Tryba, F. T. Geyling, The effects of gas phase convection on mass transfer in spin coating, Journal of Applied Physics 73 (2) (1993) 585–600.

[21] J. J. van Franeker, D. Westhoff, M. Turbiez, M. M. Wienk, V. Schmidt, R. A. Janssen, Controlling the dominant length scale of liquid–liquid phase separation in spin-coated organic semiconductor films, Advanced Functional Materials 25 (6) (2015) 855–863.

[22] F. Horowitz, E. Yeatman, E. Dawnay, A. Fardad, Real-time optical monitoring of spin coating, Journal de Physique III 3 (11) (1993) 2059–2063.

[23] D. T. Toolan, A. Dunbar, S. Ebbens, N. Clarke, P. D. Topham, J. R. Howse, et al., Direct observation of morphological development during the spin-coating of polystyrene–poly (methyl methacrylate) polymer blends, Journal of Polymer Science Part B: Polymer Physics 51 (11) (2013) 875–881.

[24] D. T. Toolan, J. R. Howse, Development of in situ studies of spin coated polymer films, Journal of Materials Chemistry C 1 (4) (2013) 603–616.

[25] S. Shiratori, D. Kato, K. Sugasawa, H. Nagano, K. Shimano, Spatio-temporal thickness variation and transient marangoni number in striations during spin coating, International Journal of Heat and Mass Transfer 154 (2020) 119678.

[26] B. Chen, Investigation of the solvent-evaporation effect on spin coating of thin films, Polymer Engineering & Science 23 (7) (1983) 399–403.

[27] P. Mokarian-Tabari, M. Geoghegan, J. Howse, S. Heriot, R. Thompson, R. Jones, Quantitative evaluation of evaporation rate during spin-coating of polymer blend films: Control of film structure through defined-atmosphere solvent-casting, The European Physical Journal E 33 (4) (2010) 283–289.

[28] D. P. Birnie, Surface skin development and rupture during sol-gel spin-coating, Journal of sol-gel science and technology 31 (1) (2004) 225–228.

[29] D. Bornside, C. Macosko, L. Scriven, Spin coating: One-dimensional model, Journal of Applied Physics 66 (11) (1989) 5185–5193.

[30] S. Eickelmann, H. Riegler, Rupture of ultrathin solution films on planar solid substrates induced by solute crystallization, Journal of colloid and interface science 528 (2018) 63–69.

[31] R. Köhler, P. Lazar, H. Riegler, Optical imaging of thin films with molecular depth resolution, Applied physics letters 89 (24) (2006) 241906.

[32] L. Manske, D. Graves, W. Oldham, Dynamic measurements of film thickness over local topography in spin coating, Applied physics letters 56 (23) (1990) 2348–2350.

[33] L. Peurrung, D. Graves, Film thickness profiles over topography in spin coating, Journal of the electrochemical society 138 (7) (1991) 2115–2124.

[34] O. S. Cregan V, A note on spin-coating with small evaporation, Journal of Colloid and Interface Science 314 (2007) 324–328.

[35] Y. Chang, W. Wu, W. Chen, Theoretical analysis on spin coating of polyimide precursor solutions, Journal of The Electrochemical Society 148 (4) (2001) F77–F81.

[36] P. Leinonen, D. Mackay, A mathematical model of evaporation and dissolution from oil spills on ice, land and under ice, Proc. 10th Canadian Symp. 1975: Water Poll. Research Canada.

[37] D. Mackay, R. S. Matsugu, Evaporation rates of liquid hydrocarbon spills on lannd and water, The Canadian Journal of Chemical Engineering 51 (1973) 434–439.

[38] F. Heymes, L. Aprin, A. Bony, S. Forestier, C. Stefano, G. Dusserre, An experimental investigation of evaporation rates for different volatile organic compounds, Process Safety Progress 32 (2) (2013) 193–198.

[39] T. Poos, E. Varju, Mass transfer coefficients for water evaporation by theoretical and empirical correlations, International Journal of Heat and Mass Transfer 153 (2020) 119500.

[40] A. C. Johnston-Peck, W. Junwei, J. B. Tracy, Formation and grain analysis of spin-cast magnetic nanoparticle monolayers, Langmuir 27 (8) (2011) 5040–5046.

[41] D. Mao, G. Lv, G. Gao, B. Fan, Fabrication of polyimide films with imaging quality using a spin-coating method for potential optical applications, Journal of Polymer Engineering 39 (10)

(2019) 917–925.

[42] I. Smallwood, Handbook of organic solvent properties, Butterworth-Heinemann, 2012.

[43] R. M. Felder, R. W. Rousseau, L. G. Bullard, Elementary Principles of Chemical Processes, Wiley Global Education, 2015.

[44] T. R. Marrero, E. A. Mason, Gaseous diffusion coefficients, Journal of Physical and Chemical Reference Data 1 (1) (1972) 3–118.

[45] H. Y. Erbil, Y. Avci, Simultaneous determination of toluene diffusion coefficient in air from thin tube evaporation and sessile drop evaporation on a solid surface, Langmuir 18 (13) (2002) 5113–5119.

[46] G. Lugg, Diffusion coefficients of some organic and other vapors in air, Analytical Chemistry 40 (7) (1968) 1072–1077.

[47] W. J. Lyman, W. F. Reehl, D. H. Rosenblatt, Handbook of chemical property estimation methods: environmental behavior of organic compounds, Washington, DC (United States); American Chemical Society, 1990.

[48] A. Berezhnoi, A. Semenov, Binary Diffusion Coefficients of Liquid Vapors in Gases, Begell House, 1997.

7. Appendix

Physico-chemical properties of the solvents

Table 1: **Physico-chemical properties of the solvents at 298,15** K. The unmarked data for density (ρ_{solv}), molecular weight (M_{solv}), kinetic viscosity (ν_{solv}), and vapor pressure P^*_{solv} (estimation by the Antoine equation) are from Ref. [42]. The data marked by * are from Ref. [43]. The data for the diffusion coefficients in air ($D_{solv,air}$) are from: ** Ref.[44], ‡ Ref.[45], † Ref.[46], ! Ref.[47], § Ref. [8], $ Ref.[48].

Solvent	$\rho_{solv}[kg/m^3]$	$M_{solv}[10^{-3}kg/mol]$	$P^*_{solv}[10^3Pa]$	$D_{solv,air}[10^{-6}m^2/s]$	$\nu_{solv}[10^{-7}m^2/s]$
Water	1000	18	3.37	25.1**	8.93
Toluene	867	92	3.79	8.03‡	6.34
Ethyl acetate	902	88	12.6	8.61†	4.72
Chloroform	1483	119	26.2	8.88†	3.65
Tetrahydrofuran	889	72	21.6	11.1§	5.17
Dimethylformamide	944	73	0.502	9.73†	8.5
n-Heptane	684	100	6.11	7.05!	5.5
n-Octane	703	114	1.86	6.16†	7.25
n-Nonane	718	128	0.572	6.43!	8.65
n-Decane	730	174	0.22	5.74!	11.8
Methylcyclohexane	770	98	6.05*	6.15$	8.7

Speed-independent evaporation rates of the solvents

Table 2: **Speed-independent evaporation rates: Experimental results (e) and calculated numbers ($\mathbf{e_{th}}$)**. The measured evaporation rates, e, are also presented in Fig. 4 of the main text. The theoretical evaporation rates, e_{th}, are calculated using Eq.(8) (see below and main text) with the physico-chemical properties given by Table 1 and with $R_g = 8.31\,\mathrm{J\,mol^{-1}\,K^{-1}}$, $\omega = 16.7\,\mathrm{s^{-1}}$ (=1000 rpm), $T = 299.15\,\mathrm{K}$ (= 26 °C), $RH_{H_2o} = (40 \pm 1)\%$.

Solvent	$e[10^{-6}m/s^{1/2}]$	$e_{th}[10^{-6}m/s^{1/2}]$
Water	0.07	0.05
Toluene	0.18	0.19
Ethyl acetate	0.61	0.58
Chloroform	1.11	1.01
Tetrahydrofuran	0.68	0.80
Dimethylformamide	0.01	0.02
n-Heptane	0.37	0.39
n-Octane	0.12	0.12
n-Nonane	0.04	0.04
n-Decane	0.01	0.02
Methylcyclohexane	0.29	0.35

Evaporation Behaviour of a Thinning Liquid Film in a Spin Coating Setup: Comparison Between Calculation and Experiment

Supplemental Material

José Danglad-Flores, Stephan Eickelmann, and Hans Riegler

February 14, 2021

1. Theoretical analysis of evaporative-hydrodynamic film thinning in a spin coating configuration

1.1. Analysis of the film thinning of a pure volatile liquid

The thinning behavior of a Newtonian, volatile liquid film of thickness h on a rotating support can be described by [1]:

$$dh/dt = -2K\,h^3 - E\,. \tag{1}$$

Eq-S. (1) assumes no slip at the liquid/substrate interface (lubrication ap-

proximation) and a free liquid surface. Film thinning due to contributions from surface tension and gravity is neglected [2, 1, 3]. The parameters characterizing the process according to Eq-S. (1) are K and E. E is the evaporation rate. K is the flow parameter. K describes the hydrodynamic behavior with $\omega =$ rotational speed, and $\nu =$ kinematic viscosity:

$$K = \omega^2/(3\nu), \tag{2}$$

For the case of a pure liquid, Kapitschka et *al.* [3] solved Eq-S. (1) by a change of variables.

$$\frac{d\xi}{d\tau} = -\xi^3 - 1, \tag{3}$$

which is obtained by rescaling, with $\xi = h/h_{tr}$ and $\tau = t/t^*_{sc}$, where:

$$h_{tr} = (E/2K)^{1/3}, \tag{4}$$

$$t^*_{sc} = (2E^2K)^{-1/3}, \tag{5}$$

are the natural scales.

h_{tr} is called the transition height. Per definition, h_{tr} marks the film thickness, where film thinning is driven equally by evaporation and by hydrodynamics. For films thicker than h_{tr}, its thinning is dominated by flow. For films thinner than h_{tr} thinning it is dominated by evaporation.

t^*_{sc} represents the *reduced* process duration. It is the absolute time from $h = h_{tr}$ to $h = 0$.

The change of variables leads to an ordinary linear differential equation, whose solution $\tau(\xi)$ is [3]:

$$\tau(\xi) = \frac{\sqrt{3}}{6}\left\{\pi + 2\arctan\frac{1-2\xi}{\sqrt{3}} + \frac{1}{\sqrt{3}}\log\frac{1-\xi-\xi^2}{(1+\xi)^2}\right\}. \tag{6}$$

The duration of the entire spin coating process is t_{sc}. Per definition, this is the time from the start of the process (at $h \to \infty$), to its end (at $h \to 0$). According to Karpitschka et *al.* [3]:

$$t_{sc} = \frac{2\pi}{3^{3/2}}(2E^2K)^{-1/3} = \frac{2\pi}{3^{3/2}} \cdot t^*_{sc} \tag{7}$$

It is found that hydrodynamic film thinning dominates always 30% of the spin cast time at the beginning of the process, from $t = 0$ to $t = t_{tr}$ (= the time when the film thinning reaches $h = h_{tr}$). The following 70% of the film thinning is dominated by evaporation (between $t = t_{tr}$ and $t = t_{sc}$, (= the time when the film thinning reaches $h \to 0$).

The following Eq.-S (8) [3] is the analytic solution to the differential Eq-S. (1)

$$t(h) = \left\{\pi\sqrt{3}+2\sqrt{3}\arctan\frac{1-2h(2K/E)^{1/3}}{\sqrt{3}}+\log\left[1-\frac{3h(2K/E)^{1/3}}{\left(1+h(2K/E)^{1/3}\right)^2}\right]\right\}/\left(6(2E^2K)^{1/3}\right), \tag{8}$$

1.2. Analysis of the film thinning of mixtures of volatile solvents and nonvolatile solutes (zero-order approach)

In most cases the purpose of spin coating is the depostion of nonvolatile material (monomers, polymers, particles, etc.) on the substrate. It is desirable to control the deposition to vary/adjust the properties of the final deposit such as its coverage or film thickness. It has been shown in detailed experimental and theoretical studies that the theoretical analysis of an evaporative-hydrodynamic film thinning of a pure liquid as it is outlined in the previous section can easily

be adjusted for this purpose [3, 4, 5]. The final coverage, Γ (deposited units per area), or the (equivalent) film thinkness, h_f (length), of a nonvolatile solute can be estimated for mixtures of volatile solvents and nonvolatile solutes according to [3]:

$$\Gamma \approx c_0 \cdot h_{tr}. \tag{9}$$

or:

$$h_f \approx x_0 \cdot h_{tr}. \tag{10}$$

According to the results presented in the main paper this means:

$$h_f \approx 0.85 \cdot x_0 \cdot \frac{\rho_{solv}}{\rho_{solute}} \cdot \left[\frac{\nu D_{solv,air}^{1/2} P_{solv}^{*} M_{solv}}{\omega^{3/2} \rho_{solv} R_g T} \right]^{1/3}. \tag{11}$$

or:

$$\Gamma_f \approx 0.85 \cdot c_0 \cdot \frac{\rho_{solv}}{\rho_{solute}} \cdot \left[\frac{\nu D_{solv,air}^{1/2} P_{solv}^{*} M_{solv}}{\omega^{3/2} \rho_{solv} R_g T} \right]^{1/3}. \tag{12}$$

Eqs.-S (9), (10), (11), and (12) assume that both, E and K are the values from the beginning of the spin coating process. For this *zero-order approximation* it is assumed that before reaching h_{tr} the viscosity does not change significantly (e.g., due to changes of the temperature or the solute concentration because of the evaporation of the solvent). It is also assumed that the evaporation rate E does not change in the thinning range between $h = h_{tr}$ and a very thin film with a thickness close to $h = h_f$ ("close" meaning at a distance much smaller than $h_{tr} - h_f$).

These assumptions may be questioned, because the solute concentation, c, *does* (of course) increase due to the evaporation of the solvent (per definition it

even increases to $c \to \infty$ for $h = h_f$). Nevertheless, as stated above already, the limits of the validity of this zero-order approximation were analyzed in detail before [4, 5],. And, for reasons presented in these studies it is found, that the evaporation rate changes rather little during by far most of the film thinning process. It only changes significantly very close to h_f.

In many cases the zero-order approximation works quantitatively quite well. With this approximation, as demonstrated in the following, it is possible to predict ab initio the experimental results of h_f. One only needs the process parameters (rotation speed, weighing in concentration, temperature) and generally available physico-chemical data of the solvents and solutes and Eq.-S (11) (or Eq.-S (12)).

2. Experimental observation of the film thinning and its relation to the calculated film thinning behavior

Figure-S 1 depicts the relation between on-line optical microscopy observations and the film thinning in a typical experiment. In this case it is a n-nonane film on a SiO_2 substrate rotating at ω=1000 rpm. The thinning behaviour (main plot on Figure-S 1) changes from a rather steep, nonlinear decrease before the transition height, h_{tr}, to a less steep, linear section after h_{tr}. The steep, nonlinear thickness decrease is dominated by flow dynamics. After h_{tr} the linear section represents the evaporative thinning regime. The thinning curve is analyzed (fitted, red solid line) according to Eq.-S(8) [3]. The fit reveals the evaporation rate E, the flow parameter K, the transition height h_{tr}, as well as the total spin coating time, t_{sc}. Please note, that the beginning of the process ($t_{sc} = 0$) is obtained

(defined) by extrapolating the fit to an initial height of $h(t=0)=\infty$ [1].

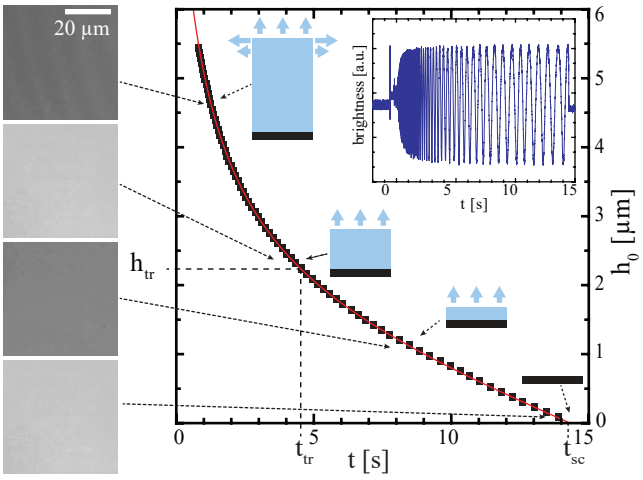

Figure 1: On-line visualization of a liquid film thinning and its corresponding thinning curve. On the left side are depicted a few images as they are obtained by optical microscopy during the film thinning. The images are essentially featureless (planar film) and differ only by their brightness as consequence of the interferences between the various interfaces (top of the film, bottom of the film, interface SiO_2/Si). The measured variation of brightness with time is depicted in the insert. These gray level variations are used to calculate the thinning curve. The resulting data (dark squares) are presented in the main plot. Depicted are real data for n-nonane on a SiO_2 substrate rotating at ω=1000 rpm. The arrows from the microscopy images to the plot indicate the time at which they were taken. Shown are also the transition height, h_{tr}, and the corresponding transition time, t_{tr}. The red solid line is the fit of the data according to Eq.-S(8). This fit reveals E, K, and h_{tr}. Extrapolation of the fit to $h \to \infty$ discloses $t=0$ and thus also the total spin cast time t_{sc} assuming $h \to 0$ at $t=t_{sc}$.

[1] A "real" initial film height, h_0, marking the beginning of the film thinnning "in reality" does not exist and cannot be defined with meaningful accuracy. Real spin coating does not start in a well-defined moment with a flat film being abruptly subject to a constant rotation causing abruptly its thinning due to viscous flow and evaporation. Typically a liquid aliquot is deposited on a (static, accelerating, constantly rotating) substrate. The rotation (and/or gravity) causes the continuous transformation of the initial (non-planar) shape of the liquid into a planar, continuously thinning film [2]. A theoretical analysis assuming h_0 as a process parameter is unlikely successful in describing a real spin coating process.

3. Application examples

For the following calculation it is assumed that $R_g = 8.31 \times 10^{-3}\,\mathrm{m^3kPa/Kmol}$ and $T = 298\,\mathrm{K}$.

3.1. Nanoparticle monolayer deposition

FePt NPs were successfully deposited in a hexagonally ordered monolayer ($\Gamma \sim 10000$ particles per μm^2) [6]. We estimate that the particle diameter is 11.2 nm (3.6 nm radius for the FePt core plus 2 nm for the stabilizing shell). The shell size, based on the dimensions of oleic acid and oleylamine [7], is confirmed by the center to center average distance between neighboring particles [6]. We approximate the particle density as $\rho_p = 12\,000\,\mathrm{kg/m^3}$ based in the mass fraction contributions. For spin casting from a dispersion in hexane at $\omega = 3000\,\mathrm{rpm}$ [6], we predict a transition height $h_{tr} \approx 13\,\mu\mathrm{m}$ (hexane properties taken from Ref. [8], with $\nu = 4.46 \times 10^{-7}\,\mathrm{m^2\,s^{-1}}$, $\rho_L = 655\,\mathrm{kg\,m^{-3}}$, $M_a = 86.18\,\mathrm{g\,mol^{-1}}$, $P^* = 20.2\,\mathrm{kPa}$, and $D_{ab} = 7.33 \times 10^{-6}\,\mathrm{m^2\,s^{-1}}$ [9]). An estimate for c_0 (in particles per volume) is obtained via Eq.-S (9). We translate this into x_0 by multiplication with the density ratio $\frac{\rho_L}{\rho_S}$ and the volume of the particles.

All this taken into account, we predict an initial concentration in the range of $x_0 = 0.01\,\mathrm{w/w}$. This agrees with the reported experimental conditions [6].

3.2. Polymer film deposition

A protocol to fabricate a polyimide films by spin casting starting from the monomer deposition has been proposed by Mao et al. [10]. The authors conducted several experiments to obtain empirical and case specific equations (their Eqs. 8 and 9 [10]).

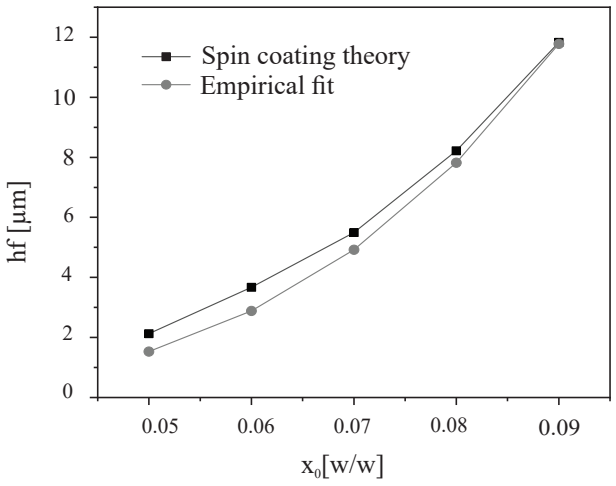

Figure 2: Final polymer film thicknesses h_f as function of x_0, the weighing in monomer mass fraction (pyromellitic in dianhydride indimethylacetamide). The gray round dots show the empirical data/fit reported by D. Mao et al.[10] (their Eq. 8 and fitted from data on their Fig. 2A). The curve with the black squares is predicted by our approach through Eq. (11).

Figure 2 depicts the final polymer film thicknesses as function of x_0, the weighing in monomer mass fraction (pyromellitic dianhydride in dimethylacetamide). The experiments were performed with $\omega = 15\,\mathrm{s}^{-1}$. The gray dots show the empirical fit based on measurements of the final film thickness as reported by Mao et al.[10] (their Eq 8 and fitted from data on their Fig 2A). The curve connecting the black squares shows our prediction according to Eq.-S (11). The properties of Dimethylacetamide were taken from Ref. [8] as $\rho_L = 945\,\mathrm{kg\,m}^{-3}$, $M_a = 87\,\mathrm{g\,mol}^{-1}$, $P^* = 0.3\,\mathrm{kPa}$ [11], and $D_{ab} = 9.73 \times 10^{-6}\,\mathrm{m}^2\,\mathrm{s}^{-1}$ (we assumed the mass diffusion coefficient in air for DMF [9] according to Table 1 Appendix). The dynamic viscosity, η_0, for each weighing in concentration was taken directly from Figure 3 of Mao et al. [10]. The kinetic viscosity, $\nu = \eta/\rho_0$, for the solution assumes a density of $\rho_0 = x_0\rho_S + (1 - x_0)\rho_L$. The density of pyromellitic dianhydride (ρ_S) was taken as $1680\,\mathrm{kg\,m}^{-3}$.

References

[1] D. Meyerhofer, "Characteristics of resist films produced by spinning," *Journal of Applied Physics*, vol. 49, no. 7, pp. 3993–3997, 1978.

[2] A. G. Emslie, F. T. Bonner, and L. G. Peck, "Flow of a viscous liquid on a rotating disk," *Journal of Applied Physics*, vol. 29, no. 5, pp. 858–862, 1958.

[3] S. Karpitschka, C. M. Weber, and H. Riegler, "Spin casting of dilute solutions: Vertical composition profile during hydrodynamic-evaporative film thinning," *Chemical Engineering Science*, vol. 129, pp. 243–248, 2015.

[4] J. Danglad-Flores, S. Eickelmann, and H. Riegler, "Deposition of polymer films by spin casting: A quantitative analysis," *Chemical Engineering Science*, vol. 179, pp. 257 – 264, 2018.

[5] J. Danglad-Flores, K. Eftekhari, A. G. Skirtach, and H. Riegler, "Controlled deposition of nanosize and microsize particles by spin-casting," *Langmuir*, vol. 35, no. 9, pp. 3404 – 3412, 2019.

[6] A. C. Johnston-Peck, W. Junwei, and J. B. Tracy, "Formation and grain analysis of spin-cast magnetic nanoparticle monolayers," *Langmuir*, vol. 27, no. 8, pp. 5040–5046, 2011.

[7] S. Mourdikoudis and L. M. Liz-Marzán, "Oleylamine in nanoparticle synthesis," *Chemistry of Materials*, vol. 25, no. 9, pp. 1465–1476, 2013.

[8] I. Smallwood, *Handbook of organic solvent properties*. Butterworth-Heinemann, 2012.

[9] G. Lugg, "Diffusion coefficients of some organic and other vapors in air," *Analytical Chemistry*, vol. 40, no. 7, pp. 1072–1077, 1968.

[10] D. Mao, G. Lv, G. Gao, and B. Fan, "Fabrication of polyimide films with imaging quality using a spin-coating method for potential optical applications," *Journal of Polymer Engineering*, vol. 39, no. 10, pp. 917–925, 2019.

[11] K. Nasirzadeh, R. Neueder, and W. Kunz, "Vapor pressures of propylene carbonate and n, n-dimethylacetamide," *Journal of Chemical & Engineering Data*, vol. 50, no. 1, pp. 26–28, 2005.